Journal of Non-Crystalline Solids 433 (2016) 68–74

Contents lists available at ScienceDirect

Journal of Non-Crystalline Solids

journal homepage: www.elsevier.com/locate/jnoncrysol

A new transition metal-tellurite glass family: Electrical and structural properties

S. Terny [a,b], M.A. De la Rubia [b], J. De Frutos [b], M.A. Frechero [a,*]

[a] INQUISUR — Universidad Nacional del Sur, Departamento de Química, Av. Alem 1253, 8000 Bahía Blanca, Buenos Aires, Argentina
[b] POEMMA-CEMDATIC, E.T.S.I. Telecomunicación, UPM, Avda. Complutense, 30, 28040 Madrid, Spain

ARTICLE INFO

Article history:
Received 7 September 2015
Received in revised form 16 November 2015
Accepted 26 November 2015
Available online 9 December 2015

Keywords:
Amorphous materials
Impedance spectroscopy
Raman spectroscopy
Ionic conductivity

ABSTRACT

Glasses of composition 0.8 [xBaO.(1 − x)MgO]. 0.2*TM*.2TeO_2 with *TM*: MoO_3, WO_3, V_2O_5 or Nb_2O_5 (x = mol content) were obtained by the melt quenching technique. Raman Spectroscopy, Density and Differential Scanning Calorimetry were used to infer their microscopic structure and electrical properties were studied using Impedance Spectroscopy. Some singularities in their electrical and structural properties appeared. Deviations from linearity as a function of alkaline-earth oxide modifier content were observed both on the electrical and structural properties. They were analyzed considering the intensity of the electrical field of the mix of alkaline earth cations which induced changes on the glassy matrix and the mixed alkaline-earth effect was considered. The observed relationships between their electrical and structural properties and the mix of alkaline earth cations were different according to the transition metal oxide present.

1. Introduction

Tellurite-based glasses are the subject of extensive research because of their electrical and optical properties. Some of their main features include extended infrared transmittance, high non-linear optical indices and low fusion temperature. Also, they constitute an excellent matrix for active element doping [1].

Many oxide glasses modified with a mix of alkali oxides exhibit a non-additive variation of certain properties. This is known as the "mixed alkali effect (MAE)" and it is still an unsolved phenomenon in glass science. The MAE especially manifests itself in non-additive discrepancies in transport properties, such as diffusion, conductivity and viscosity. These dynamical properties contrast with static properties such as density, refractive index and molar volume; all of which usually exhibit relatively small deviations from linearity [2–3].

However, there is still much to understand about the "mixed alkaline-earth effect (MAEE)". MAEE seems to be phenomenologically analogous to MAE considering that one alkaline-earth ion is partially replaced by another alkaline-earth ion. Deviations from linearity on their property behavior as a function of the alkaline-earth ratio are observed although certain dynamical properties behave differently depending on the *nature* of the glassy matrix composition and the peer of alkaline-earth cations mixed [4–16]. Since alkaline-earth cations affect the glass properties in a non-predictive manner, it is important to study this effect from both the scientific and the technological points of view.

Despite the technological and scientific relevance of tellurite glasses, so far, there is no available data of this effect in the literature. Then, the aim of this work is to study systematically the structural and electrical properties of a family of glasses of general formula: 0.8[xBaO (1 − x)MgO] 0.2*TM*. 2TeO_2 with *TM* = Nb_2O_5, V_2O_5, MoO_3 or WO_3. We carefully study how the materials' properties are affected by the partial replacement of MgO by BaO (i.e. when x mol content ➔ 0.0 the system composition is: 0.8 MgO 0.2*TM*. 2TeO_2 and when x mol content ➔ 1.0 the system composition is: 0.8 BaO 0.2*TM*. 2TeO_2) and how the structure of the glassy framework varies by changing the transition metal oxide which acts as a former-modifying oxide, considering that TeO_2 is a glass former oxide while BaO and MgO are modifier oxides. These transition metal oxides have been carefully chosen in order to change the ion size and its electronic configuration, i.e. the kind of polyhedron that each transition metal cation forms with the oxygen atoms.

2. Materials and methods

2.1. Sample preparation

The samples were prepared by a standard melt quenching technique using reagent grade chemicals of TeO_2, $MgCO_3$, $BaCO_3$, MoO_3, WO_3, Nb_2O_5 and V_2O_5. Starting from the nominal composition expressed through the general formula, every component (all of chemical grade; 99.9%) was properly weighted with a laboratory scale sensitive to 0.1 mg in order to obtain (10.00 ± 0.01) g of each sample. Next, the components were well mixed and placed in an alumina crucible and the carbonate decarboxylation process (when carbonates were used)

* Corresponding author.
E-mail address: frechero@uns.edu.ar (M.A. Frechero).

http://dx.doi.org/10.1016/j.jnoncrysol.2015.11.030
0022-3093/

was made at a lower temperature than the mix melting point. When the effervescence finished, the mix was heated to reach 1323 K and after that, it was held for an hour in an electric furnace. During the process, the crucible was shaken frequently to ensure homogenization. Then, the molten material was poured on a preheated aluminum plate in form of drops and held for annealing at 523 K during 2 h.

2.2. X-ray diffraction analysis (XRD)

The amorphous character of the samples was tested by X-Ray Diffraction. The XRD patterns of powdered samples after the annealing were collected with a Bruker D8 Advance Diffractometer at continuous scan mode with a copper anode and 45 kV–30 mA for the tension and electrical current generator respectively. The samples were exposed to the Cu K_α radiation ($\lambda = 1.54$ Å) at room temperature in the 2θ range: 10°–60°.

2.3. Glass transition temperature and isobaric heat capacity

DSC curves were recorded during heating rates using a SDT-Q600 calorimeter. We search the glass transition temperature (T_g) of each sample with a heating rate of 10 $K \cdot min^{-1}$, starting from room temperature up to 600 °C, using 15–20 mg of glass samples previously crashed in an agate mortar. The T_g values were obtained from the middle point of the C_p jump during the heating. The associated upper-limit error of the temperature measurements is an interval of one degree according to the middle point procedure with the TQA software. The heat capacity change at glass transition ($\Delta C_{p(Tg)}$) was measured from the DSC thermogram for each composition.

2.4. Vickers micro-hardness

Every glass sample was mirror like polished and Vickers microhardness (H_V) was measured using a Duramin 5 indenter (Struers A/S). A total of 34 indents were conducted on each sample using an indentation time of 0.05 s and an indentation load of 500 mN. The measurements were performed in a regular atmosphere, i.e. air (no gas composition controlled) at room temperature.

2.5. Structural aspects

Raman spectra were collected at room temperature on glass samples in the 0–4000 cm^{-1} range using a Raman spectrometer with a 532 nm green laser as the probing light source. The sample focalization was done using a microscope with a ×20 objective. The measurements were performed using a laser power of 42 mW in order to avoid damage or localized heating of the glasses. The obtained spectra were deconvoluted using Gaussian fitting to determine the Raman peak positions.

2.6. Electrical characterization

The samples were polished with very fine sand papers in order to obtain glass disks with two parallel faces with thickness ranging

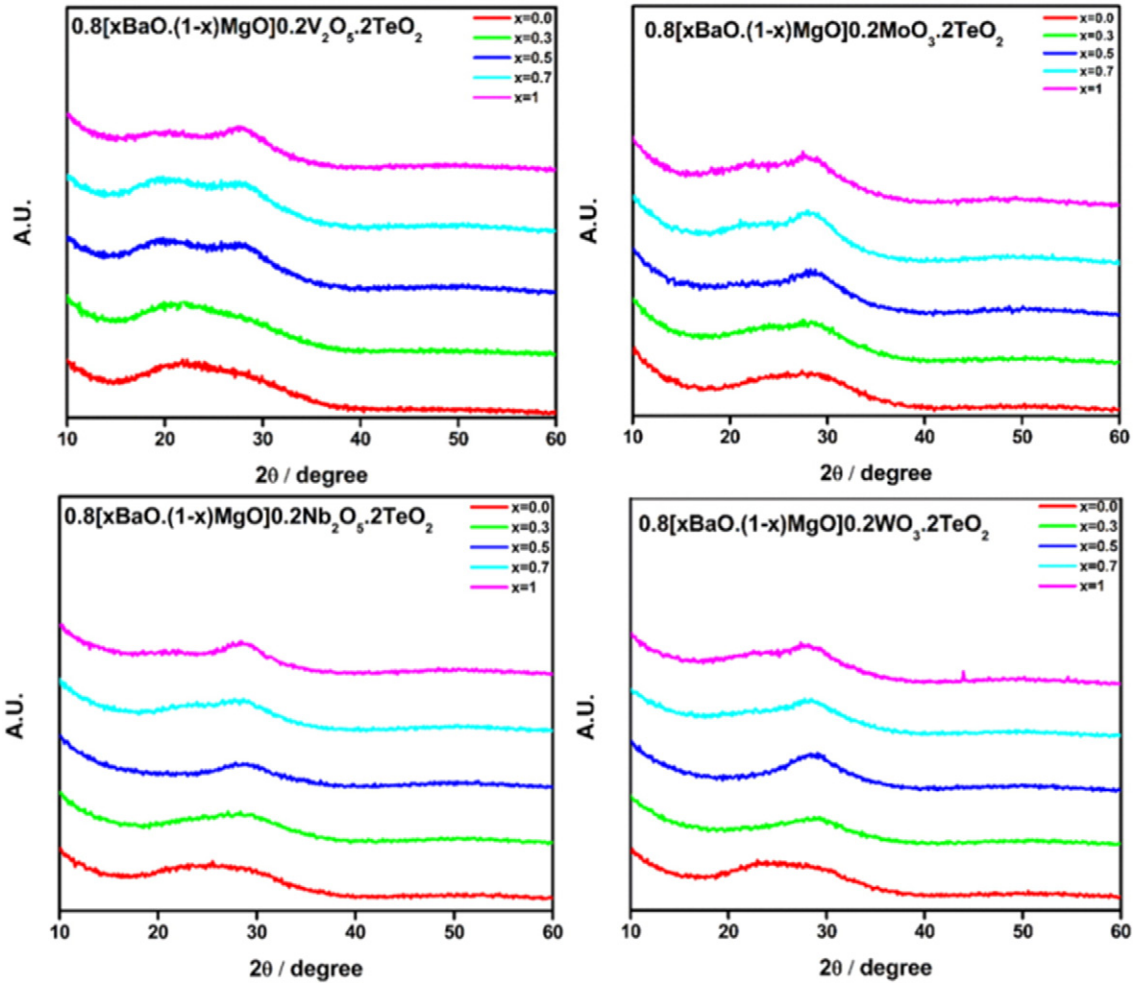

Fig. 1. XRD patterns for each composition of every studied system.

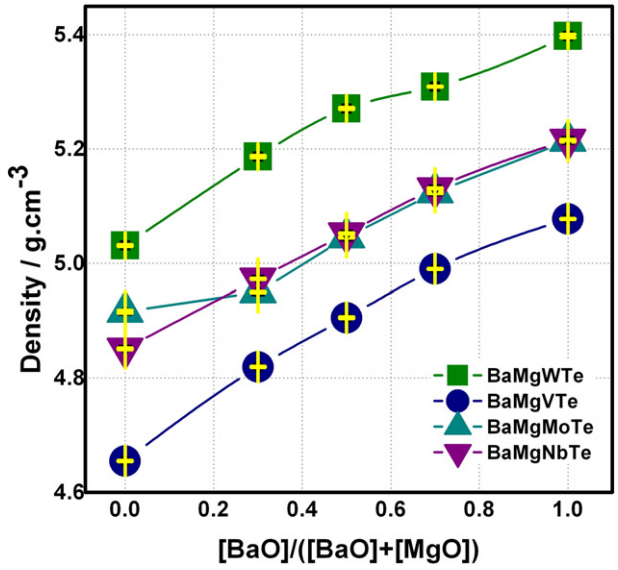

Fig. 2. Density values as function of the molar ratio [BaO]/([BaO] + [MgO]) for every composition of each glass family.

between 0.5 and 0.7 mm. Each sample was coated uniformly with a thin layer of silver paint with the purpose of having proper electrical contact. For the impedance determinations, a Solartron Impedance Analyzer (model 1260) with a 1296A dielectric interface was used in the frequency range 1.10^{-2} Hz–1.10^{7} Hz with an AC voltage amplitude of 1 V. For each composition the spectra were carried in a temperature range starting at 100 °C up to a temperature of 15 °C below T_g.

2.7. Density measurements

Room-temperature densities of the glasses were determined by Archimede's principle using water as the immersion liquid, being the informed values the average of three independent density measures.

Table 1
Glass composition, ratio of alkaline earth oxides, OPD and V_M values for every composition of each glass family.

Glass composition	Ratio [BaO]/([BaO] + [MgO])	OPD/Oxy. mol.dm^{-3} ± 0.01	V_M/cm^3 ± 0.01
0.8MgO.0.2V_2O_5.2TeO_2	0.0	69.61	27.70
0.8[0.3BaO.0.7MgO].0.2V_2O_5.2TeO_2	0.3	56.91	28.69
0.8[0.5BaO.0.5MgO].0.2V_2O_5.2TeO_2	0.5	48.71	29.42
0.8[0.7BaO.0.3MgO].0.2V_2O_5.2TeO_2	0.7	40.93	30.13
0.8BaO.0.2V_2O_5.2TeO_2	1.0	29.72	31.39
0.8MgO.0.2Nb_2O_5.2TeO_2	0.0	69.54	27.80
0.8[0.3BaO.0.7MgO].0.2Nb_2O_5.2TeO_2	0.3	56.44	28.93
0.8[0.5BaO.0.5MgO].0.2Nb_2O_5.2TeO_2	0.5	48.29	29.67
0.8[0.7BaO.0.3MgO].0.2Nb_2O_5.2TeO_2	0.7	40.57	30.39
0.8BaO.0.2Nb_2O_5.2TeO_2	1.0	29.49	31.63
0.8MgO.0.2MoO_3.2TeO_2	0.0	69.83	25.78
0.8[0.3BaO.0.7MgO].0.2MoO_3.2TeO_2	0.3	54.69	27.43
0.8[0.5BaO.0.5MgO].0.2MoO_3.2TeO_2	0.5	46.26	28.10
0.8[0.7BaO.0.3MgO].0.2MoO_3.2TeO_2	0.7	38.13	28.85
0.8BaO.0.2MoO_3.2TeO_2	1.0	26.59	30.08
0.8MgO.0.2WO_3.2TeO_2	0.0	68.30	26.35
0.8[0.3BaO.0.7MgO].0.2WO_3.2TeO_2	0.3	54.93	27.31
0.8[0.5BaO.0.5MgO].0.2WO_3.2TeO_2	0.5	46.41	28.01
0.8[0.7BaO.0.3MgO].0.2WO_3.2TeO_2	0.7	38.00	28.95
0.8BaO.0.2WO_3.2TeO_2	1.0	26.54	30.15

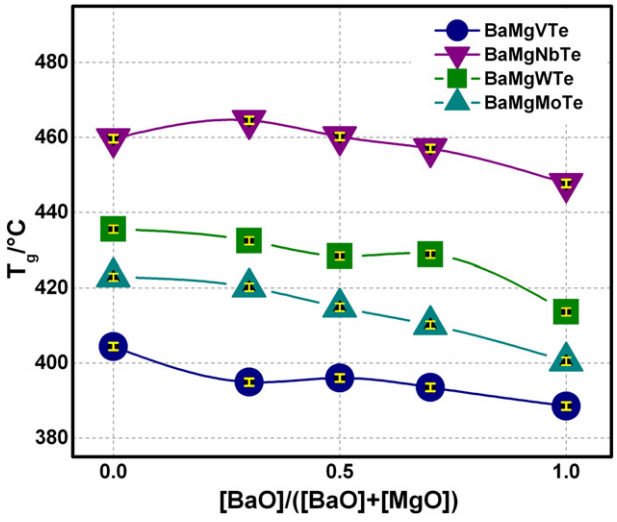

Fig. 3. T_g values as function of the molar ratio [BaO]/([BaO] + [MgO]).

3. Results

3.1. X-ray diffraction

The amorphous state of the obtained samples was analyzed with XRD and DSC. Fig. 1 shows the XRD patterns which confirm the glassy nature of the samples as none of them exhibit sharp intense peaks. A gradual emergence of two regions with increasing content of BaO is observed. This behavior suggests that the glassy matrix mid-range structural arrangement is different when the content of BaO is high which is not the same for every transition metal oxide in the glassy matrix. Throughout the XRD, the molybdenum glass family shows the lowest when changing the alkaline-earth oxide.

3.2. Density and oxygen packing density

Fig. 2 shows the density value for every composition as a function of the molar ratio BaO/(BaO + MgO). We observe in every case an increment in density values as the ratio tends to 1 (when only BaO is present).

On the other hand, when we compare the effect induced by the transition metal oxide incorporated in each glassy matrix, we see a major increment — near 8.32% — along the system [BaMg-**V**-Te]. Additionally, from these density values we estimate the molar volume

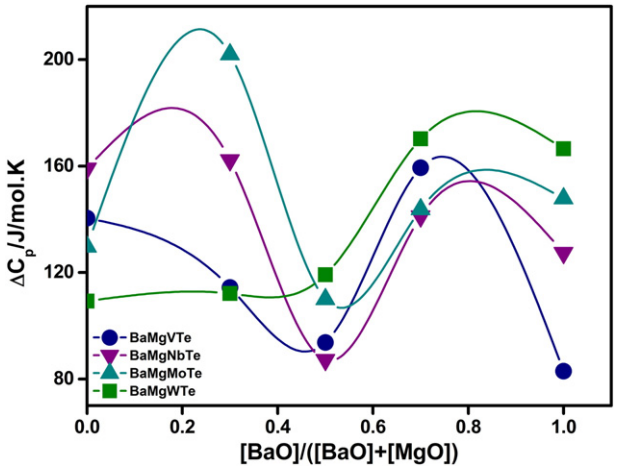

Fig. 4. $\Delta C_{p(Tg)}$ values as function of the molar ratio [BaO]/([BaO] + [MgO]).

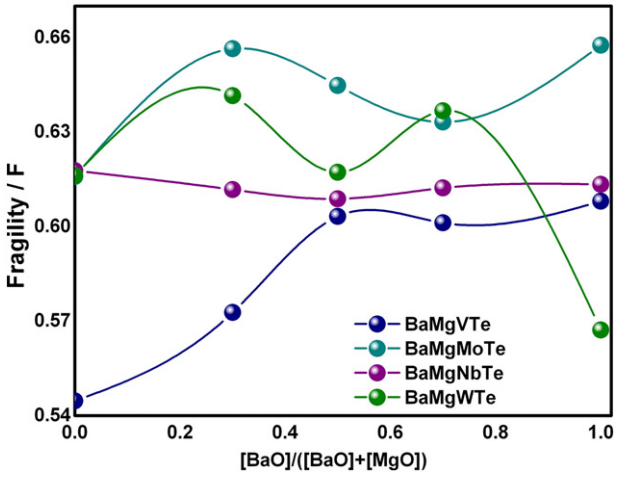

Fig. 5. Fragility parameter as function of the molar ratio [BaO]/([BaO] + [MgO]).

($V_m = M_m/\delta$) and the oxygen packing density (OPD = oxygen mol number/V_m). Both, OPD and V_m, values are listed in Table 1. From the data in this table, we notice that V_m values increase and OPD values decrease with the increasing of the BaO content. However, the effect on the OPD is more pronounced when the transition metal oxide is MoO_3 or WO_3 (elements from periodic table group VI).

3.3. Transition temperature, heat capacity and thermodynamic fragility

Fig. 3 shows the glass transition temperature (T_g) as a function of the molar ratio [BaO]/([BaO] + [MgO]). These were obtained as the temperature of the middle point in the jump of the C_p during the heating. This Fig. shows a decrease in the T_g value as the BaO content increases, no matter which transition metal oxide is present in the glassy matrix. But, this diminution is very small, only about 2–3%. Additionally, Fig. 4 shows the $\Delta C_{p(Tg)}$ values as a function of the molar ratio [BaO] / ([BaO] + [MgO]). We observe in this Fig. a stronger non-linear behavior in comparison to the T_g behavior.

The thermodynamic fragility *F* is calculated through the formula:

$$F = \left(\frac{0.151 - x}{0.151 + x}\right) \tag{1}$$

where $x = \Delta T_g / T_g$ [17]. Fig. 5 shows the variation of thermodynamic fragility parameter *F* as a function of the molar ratio [BaO] / ([BaO] + [MgO]) of each system. Once again, a strong non-linear effect on its behavior is observed except in the case of niobium family.

3.4. Vickers micro-hardness

Vickers hardness (H_V) is determined by using the micro-indentation method. Every micro-indentation experimenthas been performed on the same indenter with the same indentation load and time (500 mN and 0.05 s) ensuring crack free indents. Fig. 6*a* shows Vickers micro-hardness plotted as a function of the molar ratio [BaO] / ([BaO] + [MgO]) and Fig. 6b the indentation images of each of the highest content BaO system.

3.5. Structural results

A Raman spectrum of every composition was performed at room temperature in the range of 0–4000 cm^{-1}. Through the results we were able to find the fundamental bands which belong to the polyhedrons that build the structure of the glassy matrices. Fig. 7 shows the band at $\approx$670 cm^{-1} which varies the most when magnesium oxide is replaced progressively by barium oxide. According to the literature [1, 18,25–29] this band is associated with Te–O stretching vibration of TeO_4 in triangular bipyramidal units (tbp). In that figure a clear non-linear behavior is observed on the four glassy matrices studied in the present work. The strongest variations are observed for vanadium and molybdenum families.

3.6. Electrical characterization

In order to study the characteristics of the electrical behavior, the impedance (Z) and the phase angle (φ) of every sample has been measured as function of frequency at each temperature in the corresponding range as it was pointed out before. The electrical conductivity measured rises with increasing temperature and we can represent this behavior through the Arrhenius-type equation as:

$$\sigma_{dc} = \frac{\sigma_0}{T} . e^{-E_a / kT} \tag{2}$$

where E_a is the activation energy of the conductivity process, σ_0 is the pre-exponential factor; *k* and T have their usual meaning.

Fig. 8 a, b, c and d shows the electrical conductivity of the four systems [BaMg-**V**-Te; BaMg-**Nb**-Te; BaMg-**Mo**-Te; BaMg-**W**-Te] in an Arrhenius plot, according to Eq. (2). We noticed in those figures that

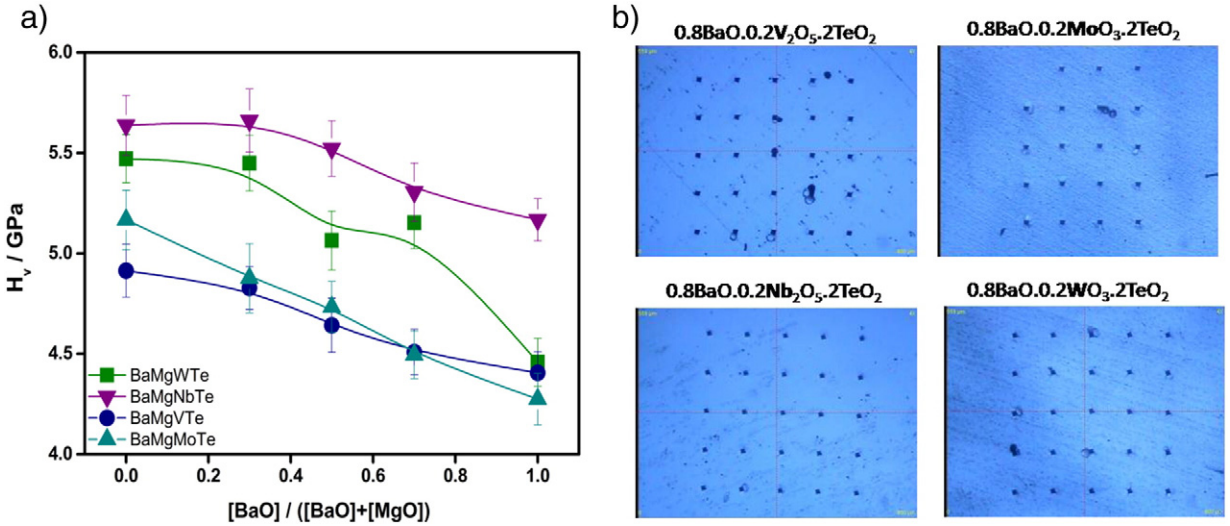

Fig. 6. a) Vickers micro-hardness (H_v) as a function of the molar ratio [BaO] / ([BaO] + [MgO]); b) indentation images of each of the highest content BaO system.

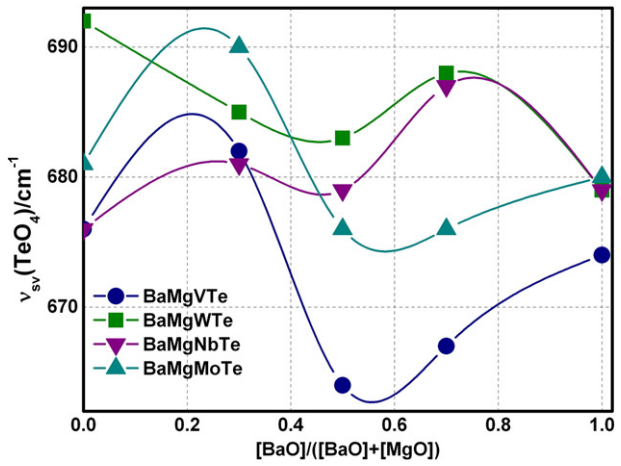

Fig. 7. Peak position wave number (ν) of the Raman signal near 670 cm^{-1} as a function of the molar ratio [BaO] / ([BaO] + [MgO]).

there is only one slope for each composition curve and this can be interpreted as the samples having single activation energy.

Fig. 9 shows the electrical conductivity isotherms at T = 500 K. We see in this fig. that the conductivity values augment as BaO content increases. But, in the case of this electrical property, the non-linearity behavior is more marked on the Vanadium and Molybdenum families. While, in the Niobium and Wolframium families the effect is quite small or almost imperceptible.

Fig. 10 shows the E_a as a function of the molar ratio [BaO] / ([BaO] + [MgO]). From this, we learn that the values diminish as BaO content increases showing in every case a deviation from linearity. Here, we notice also that BaMg**V**Te family is the one that shows smaller values than the other three.

4. Discussion

The only magnesium containing glass has for every tellurite family lower density and smaller molar volume compared to the barium containing glass respectively (Fig. 2 and Table 1). When Mg^{2+} is partially substituted by Ba^{2+} (which has a higher atomic weight) the glass density increases as it is expected. But, the difference in the molar volumes reflects a modification of the glass network structure. Molar volume diminishes by a tighter binding of oxygen to magnesium compared to barium.

The behavior of V_M (Table 1) indicates that an expansion of the glass network has taken place due to the partial substitution of MgO by BaO. This has been confirmed by the behavior of the oxygen density packing (Table 1) which decreases with increasing MgO substitution level. Then, when V_M increases due to an expansion of the glass network and OPD decreases a consequent increment in the free volume is obtained. This phenomenon has been related to differences in the field strength and polarizing power of the exchanged cations. Thus, when Mg^{2+} is substituted by a cation with lower field strength and polarizing power, such as Ba^{2+}, V_M increases probably due to a weaker attraction between the latter cations and the non-bridging oxygens (NBOs). In other words, the expansion and the concomitant decrease in compactness suffered by the glass structure have both been caused by an increased distance between the modifying cations and the NBOs. The fact that the largest increase in V_M corresponds to the addition of pure Ba^{2+}, which is the cation that has the smallest field strength, agrees with the findings of Barbieri et al. [20], who observed that V_M decreases when Ba^{2+} is substituted by other cations with higher field strength (Fe^{3+}, Cu^{2+} and Mn^{2+}).

Furthermore, in Fig. 3, we see for all the studied glasses, a non-linear behavior in glass transition temperature (T_g) when MgO is partially substituted by BaO. This figure shows that T_g tends to decrease with increasing content of BaO.

In addition to that, considering that the total concentration of the exchanged divalent modifier cations (Mg^{2+} and Ba^{2+}) was kept constant at all times, with variations only in their relative proportions, it indicates together with the fact that the concentration of the other glass constituents was not varied, that the number of NBOs could be safely assumed to be constant in our glasses. Thus, the decrease in T_g observed here with increasing BaO content cannot be attributed to a reduction in the level of association of the glass network or to the creation of an increased number of NBOs. Then, it seems to be reasonable to assume that the trends observed in the values of V_M and OPD indicate that a change in the field strength of the cations is an important factor to determine the behavior of T_g.

The liquid fragility is closely related to the microstructure of glasses and liquids. Usually for oxide compositions, at temperatures above T_g,

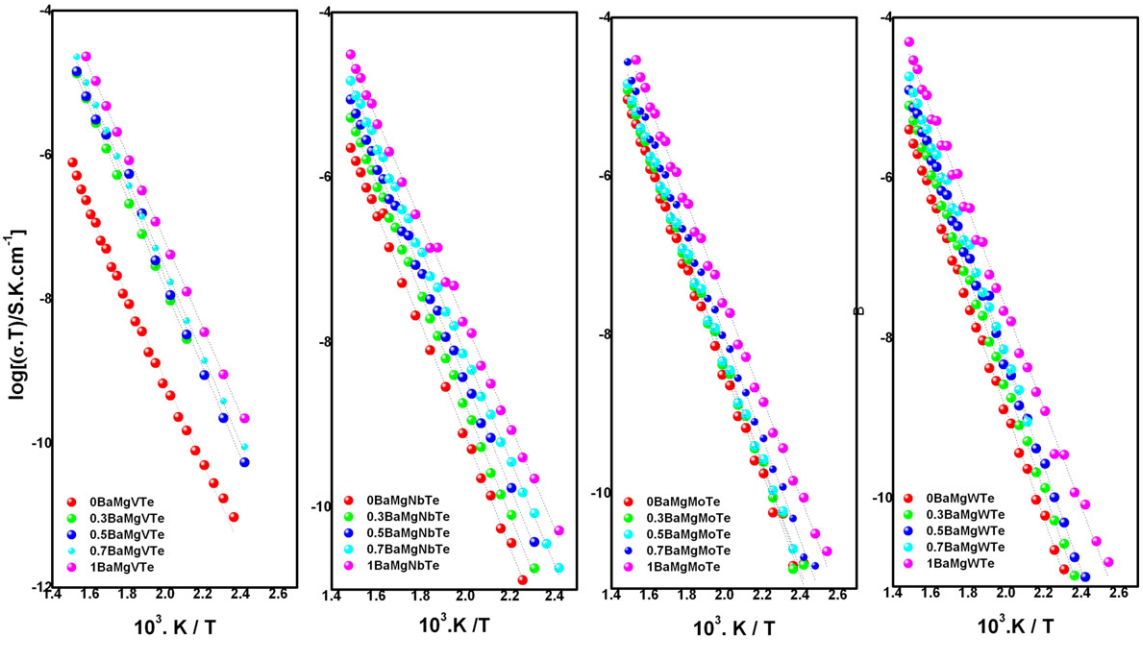

Fig. 8. Arrhenius plots of measured conductivity of every composition of each system.

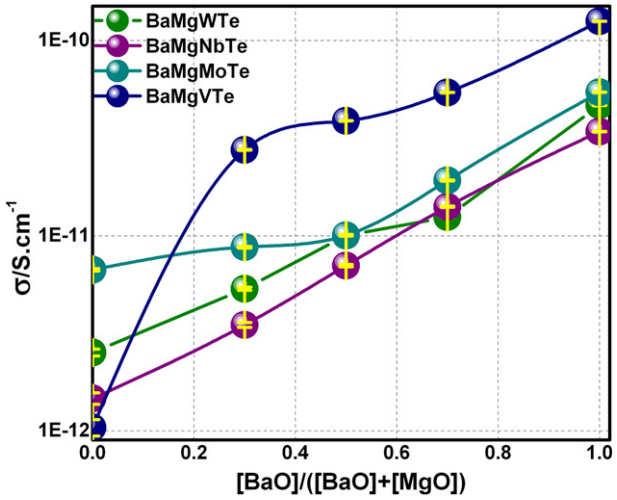

Fig. 9. Variation of electrical conductivity (T = 500 K) as a function of molar ratio of [BaO] / ([BaO] + [MgO]).

strong liquids contain a high degree of connectivity and fragile ones, a comparably low degree of connectivity [20]. More precisely, strong liquids have a medium-range structure which is more stable towards temperature fluctuation around T_g. As shown in Fig. 5, the thermodynamic fragilities exhibit an increase around x = 0.5 of cation ratio, except for the system with WO_3, in its composition which reaches a minimum. As discussed above, the highest field strength of magnesium increases the amount of rigid constraints at T_g and hence, it results in lower fragility indices when the cation ratio x ➔ 0. This is supported by the Raman spectroscopic data which implies stronger bonding in the magnesium end-member composition.

The magnitude of heat capacity that jumps at T_g is generally indicative of the nature of bonding in a material. Open-network liquids such as SiO_2 and GeO_2 which are denominated strong liquids in Angell's classification, typically display a very small jump in the heat capacity at T_g. The denominated fragile liquids, show large jumps. Fragile liquids have glassy structures that may easily reorganize through fluctuations. Strong liquids, on the other hand, intrinsically resist structural changes and show little reorganization even over wide temperature ranges [21,22]. In Fig. 4, we can observe that ΔC_p values show a minimum around cation ratio of x = 0.5. This suggest that the bonds of the magnesium and barium in the middle of cation concentration has strong

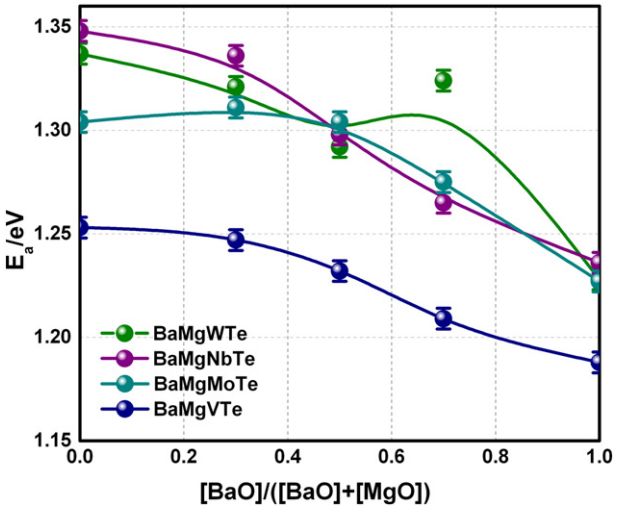

Fig. 10. Activation energy as a function of molar ratio of [BaO] / ([BaO] + [MgO]).

liquid features than the other cation ratios, except for Ba**V**Te composition that reaches a lower value when x ➔ 1 [23,24].

Fig. 6 shows the micro-hardness results and from the values this Figure shows a quasi linear behavior with the ratio of cation content. Glasses with higher field strength of modifier ions, like Mg^{2+} in the studied systems in this work, have a more rigid structure and therefore show higher values of hardness.

In Fig. 7, we see a minimum in the peak band position of TeO_4 (tbp) when cation ratio is close to 0.5. Since the oxygen coordination number for Mg^{2+} is lower than that for Ba^{2+} [22], the number of affected oxygen ions in the TeO_4 network increases when the BaO content increases. This explains why the concentration of T—O—T bonds (T = tetrahedral unit) decreases as barium BaO content increases. It is also well established that the tetrahedrally coordinated Mg^{2+} can even act as network former, contributing to an increased population of T—O—T bonding at higher magnesium content [19], and that is what we see when in the range x = 0.3 to x = 0.0.

Fig. 8 shows the Arrhenius type plots for every composition. From the linear fitting of conductivity data, we obtain a quite well adjustment that indicates a single slope for every composition, which means that unique activation energy (Fig. 10) for the migration process is present. Therefore, in the conduction isotherm at 500 K (Fig. 9) we see that the progressive replacement of MgO by BaO leads to an increase in their total conductivity values. Considering the conductivity values of both systems at the extremes when only one of the modifier oxides is present (MgO or BaO) the conduction mechanism of both modified systems with only one alkaline earth oxide is analyzed in deep detail in Refs. [23,24] and taking into account that both the T_g and OPD values decrease, it can be thought that increasing the BaO content creates a less tight and packed structure which provides greater mobility to the larger cation. It should be noted that in the conduction isotherm a deviation from linearity more evident in the BaMg**V**Te and the BaMg**Mo**Te systems suggest the existence of the MAEE. Unfortunately, MAEE in glasses have involved less attention than MAE glasses and much less on glassy matrices different to silicate glasses. Thus, what is reported up to now is that MAEE is qualitatively similar mixed alkali effect although it is less quantitatively pronounced. One of the explanation lies on the lower mobility of the bivalent alkaline earth cations than alkaline cations which move among a variety of sites because of the rearrangement in a glassy matrix [14].

5. Conclusions

We have studied the effect of the partial replacement of two alkaline-earth oxides (MgO and BaO) in four series of tellurite glasses. The Mixed Alkaline-Earth Effect is qualitatively similar to the well-known Mixed Alkali Effect but is less evident. The Mixed Alkaline-Earth Effect manifests itself as a deviation from linearity in properties like density, T_g, ΔCp, fragility, Raman peak band position, Vickers micro-hardness, conductivity and activation energy values.

On the other hand, we have explored the influence on their glass properties when the transition metal oxide is changed. Our results show that even in transition metal ions with similar electronic configuration the resulting glasses have differences in their structure and transport properties.

Acknowledgments

The authors acknowledge ARCOIRIS ERASMUS MUNDUS ACTION 2 Lot 16A (Argentine) for the scholarship and financial support by CONICET (2013-2015GI) and Universidad Nacional del Sur (PGI-2014-24/Q061).

S.T. is fellowship of the CONICET, Argentine and M.A.F is CONICET Researcher Fellow.

References

[1] G. Upender, V.G. Sathe, V.C. Mouli, Raman spectroscopic characterization of tellurite glasses containing heavy metal oxides, Physica B 405 (2010) 1269.
[2] Y. Gao, C. Cramer, Mixed cation effects in glasses with three types of alkali ions, Solid State Ionics 176 (2005) 921.
[3] A. Mohajerani, J.W. Zwanziger, Mixed alkali effect on Vickers hardness and cracking, J. Non-Cryst. Solids 358 (2012) 1474.
[4] K. Hirao, M. Yoshimoto, N. Soga, K. Tanaka, Densification of magnesium and calcium metaphosphate glasses, J. Non-Cryst. Solids 130 (1991) 78.
[5] K.-D. Kim, Influence of BaO/(SrO + BaO) on some thermal properties of R_2O-RO-SiO_2 glasses for plasma display panel substrate, Glastech. Ber. Glass. Sci. Technol. 72 (1999) 393.
[6] M. Solvang, Y.Z. Yue, S.L. Jensen, The effects of Mg–Ca and Fe–Mg substitution on rheological and thermodynamic properties of aluminosilicate melts, J. Non-Cryst. Solids 345 & 346 (2004) 782.
[7] J. Kjeldsen, M. Smedskjaer, J. Mauro, R. Youngman, L. Huang, Y. Yue, Mixed alkaline earth effect in sodium aluminosilicate glasses, J. Non-Cryst. Solids 369 (2013) 61.
[8] M.M. Smedskjaer, L. Huang, G. Scannell, J.C. Mauro, Elastic interpretation of the glass transition in aluminosilicate liquids, Phys. Rev. B 85 (2012) 144203.
[9] S. Yoshida, J.-C. Sanglebæuf, T. Rouxel, Quantitative evaluation of indentation-induced densification in glass, J. Mater. Res. 20 (2005) 3404.
[10] B.Z. Pevzner, V.P. Klyuev, Manifestation of the mixed-cation effect in dilatometric properties of RO (R_2O)–$2B_2O_3$ borate glasses upon replacement of Na_2O by BaO, Na_2O by MgO and BaO by MgO, Glas. Phys. Chem. 30 (2004) 506.
[11] L. Pavic, A. Moguš-Milankovic, P. Raghava, A. Šantic, V. Ravi, N. Veeraiah, Effect of alkali-earth modifier ion on electrical, dielectric and spectroscopic properties of Fe_2O_3 dopedNa_2SO_4–MO–P_2O_5 glass system, J. Alloy. Compd. 604 (2014) 352.
[12] S. Liu, G. Zhao, H. Ying, J. Wang, G. Han, Effects of mixed alkaline earth oxides additive on crystallization and structural changes in borosilicate glasses, J. Non-Cryst. Solids 354 (2008) 956.
[13] R. Kirchheim, On the mobility of alkaline earth ions in mixed alkali alkaline earth silicate glasses, J. Non-Cryst. Solids 328 (2003) 157.
[14] B. Roling, M.D. Ingram, Mixed alkaline-earth effects in ion conducting glasses, J. Non-Cryst. Solids 265 (2000) 113.
[15] M. Garza, J. Lópes-Cuevas, C.A. Gutierrez-Chavarría, J.C. Rendón-Angeles, J.F. Valle-Fuentes, Study of a mixed alkaline–earth effect on some properties of glasses of the CaO–MgO–Al_2O_3–SiO_2 system, Bol. Soc. Esp. Ceram. 46 (2007) 153.
[16] U. Hoppe, G. Walter, R. Kranold, D. Stachel, A. Barz, X-ray-diffraction study on the mixed alkali-alkaline earth effect in Ba, Nameta-phosphate glasses, J. Non-Cryst. Solids 224 (1998) 153.
[17] K.J. Rao, Structural Chemistry of Glasses, Elsevier Science & Technology Books, 2002 ISBN: 0080439586. Chapter 3.
[18] B.N. Nelson, G. Exarhos, Vibrational spectroscopy of cation-site interactions in phosphate glasses, J. Chem. Phys. 71 (1979) 2739.
[19] S. Sen, H. Maekawa, G.N. Papatheodorou, Short-range structure of invert glasses along the pseudo-binary join $MgSiO_3$–Mg_2SiO_4: Results from ^{29}Si and ^{25}Mg MAS NMR Spectroscopy, J. Phys. Chem. B113 (2009) 15243.
[20] L. Barbieri, S. Bruni, F. Cariati, C. Leonelli, G.C. Pellacani, C. Siligardi, U. Russo, Influence of some transition metal cations on the properties of BaO-containing glasses and glass-ceramics, Mater. Res. Bull. 34 (1999) 12–131825.
[21] C.A. Angell, Formation of glasses from liquids and biopolymers, Science 267 (1995) 1924.
[22] D. Souri, Fragility, DSC and elastic moduli studies on tellurite–vanadate glasses containing molybdenum, Measurement 44 (2011) 1904.
[23] C.S. Terny, E.C. Cardillo, P.E. diPrátula, M.A. Villar, M.A. Frechero, Electrical response of bivalent modifier cations into a vanadium–tellurite glassy matrix, J. Non-Cryst. Solids 387 (2014) 107.
[24] S. Terny, M.A. De La Rubia, S. Barolin, R.E. Alonso, J. De Frutos, M.A. Frechero, Comportamiento eléctrico de vidrios funcionales con base en TeO_2, Bol. Soc. Esp. Ceram. Vidrio 531 (2014) 15.
[25] V. Kamalaker, G. Upender, C. Ramesh, V. Chandra Mouli, Raman spectroscopy, thermal and optical properties of TeO_2–ZnO–Nb_2O_5–Nd_2O_3 glasses, Spectrochim. Acta, Part A 89 (2012) 149.
[26] F.C. Cassanjes, Y.Y. Messaddeq, L.F.C. de Oliveira, L.C. Courrol, L. Gomes, S.J.L. Ribeiro, Raman scattering, differential scanning calorimetry and Nd^{3+} spectroscopy in alkali niobium tellurite glasses, J. Non-Cryst. Solids 247 (1999) 58.
[27] T. Hayakawa, M. Hayakawa, M. Nogami, P. Thomas, Nonlinear optical properties and glass structure for MO–Nb_2O_5–TeO_2 (M═Zn, Mg, Ca, Sr, Ba) glasses, Opt. Mater. 32 (2010) 448.
[28] G. Upender, S. Bharadwaj, A.M. Awasthi, V.C. Moulia, Glass transition temperature-structural studies of tungstate tellurite glasses, Mater. Chem. Phys 118 (2009) 298.
[29] A.E. Ersundu, M. Celikbilek, N. Solak, S. Aydin, Glass formation area and characterization studies in the CdO–WO_3–TeO_2 ternary system, J. Eur. Ceram. Soc. 31 (2011) 2775.